

4-25-1988

## Surface and Sub-Surface Composition and Properties of Ion-Bombarded Lithium Alloys

A. R. Krauss

*Argonne National Laboratory*

D. M. Gruen

*Argonne National Laboratory*

N. Q. Lam

*Argonne National Laboratory*

A. B. DeWald

*Georgia Institute of Technology*

M. G. Valentine

*Georgia Institute of Technology*

*See next page for additional authors*

Follow this and additional works at: <https://digitalcommons.usu.edu/microscopy>



Part of the [Biology Commons](#)

---

### Recommended Citation

Krauss, A. R.; Gruen, D. M.; Lam, N. Q.; DeWald, A. B.; Valentine, M. G.; Sagara, A.; and Kamada, K. (1988) "Surface and Sub-Surface Composition and Properties of Ion-Bombarded Lithium Alloys," *Scanning Microscopy*: Vol. 2 : No. 3 , Article 13.

Available at: <https://digitalcommons.usu.edu/microscopy/vol2/iss3/13>

This Article is brought to you for free and open access by the Western Dairy Center at DigitalCommons@USU. It has been accepted for inclusion in Scanning Microscopy by an authorized administrator of DigitalCommons@USU. For more information, please contact [digitalcommons@usu.edu](mailto:digitalcommons@usu.edu).



---

# Surface and Sub-Surface Composition and Properties of Ion-Bombarded Lithium Alloys

## Authors

A. R. Krauss, D. M. Gruen, N. Q. Lam, A. B. DeWald, M. G. Valentine, A. Sagara, and K. Kamada

## SURFACE AND SUB-SURFACE COMPOSITION AND PROPERTIES OF ION-BOMBARDED LITHIUM ALLOYS

A.R. Krauss\*<sup>†</sup>, D.M. Gruen<sup>†</sup>, N.Q. Lam<sup>†</sup>, A.B. DeWald<sup>††</sup>, M.G. Valentine<sup>††</sup>, A. Sagara<sup>†††</sup> and K. Kamada<sup>†††</sup>

<sup>†</sup>Argonne National Laboratory, Argonne, IL, USA

<sup>††</sup>Georgia Institute of Technology, Atlanta, GA, USA

<sup>†††</sup>Nagoya University, Nagoya, Japan

(Received for publication July 26, 1987, and in revised form April 25, 1988)

### Abstract

Lithium-bearing alloys such as Si-Li, Al-Li and Cu-Li are of importance in a variety of technological applications, many of them depending on the fact that the surface composition of these alloys differs significantly from that of the bulk, both at thermal equilibrium and under ion bombardment. During ion sputtering, these materials exhibit a variety of phenomena which affect the surface composition and concentration depth profile in a complex manner. We present here experimental measurements of the surface and near-surface composition profiles of sputtered Cu-Li and Al-Li alloys. The experimental results are interpreted in terms of surface loss and radiation-induced segregation processes. Emphasis is placed on the use of these materials for use as plasma-interactive components in magnetic-confinement fusion applications.

### Introduction

Lithium-bearing alloys have a number of important technological applications. Dilute alloys of Li in Si have been used to make efficient, very rugged photocathodes [15]. More concentrated Si-Li alloys are being used as the negative electrode in advanced secondary batteries [19]. In this application, alloys containing up to 94 at.% Li have been used to contain the lithium electrode material in solid form.  $\beta$ -phase Li-Al (47-55 at.% Li) is another contender for the cathode material because of the exceptionally high diffusivity of Li in the solid [24] (~4 orders of magnitude higher than the low concentration  $\alpha$  phase) even though the cell potential is somewhat lower [19]. Depletion of the lithium inventory in these electrode materials during use is a major factor determining the life of the cell.

Lower concentration Al-Li alloys are of interest as a very light, high-strength structural material for airframe use [23]. A major consideration for this application concerns embrittlement and loss of lithium in the near-surface region as a result of welding. The mechanical properties depend on the extent of lithium loss, the depth of the depleted region, and the depth profile of the lithium concentration.

In another application, aluminum alloys have been proposed as a tokamak first-wall material [10] because of the low activation cross section for 14.1 MeV fusion neutrons. It has been found that the addition of up to 16 at.% lithium drastically reduces the neutron swelling of Al-Mg alloys [1], resulting in a material which eliminates one of the major problems of the fusion environment.

Another major problem associated with plasma-interactive materials in fusion applications concerns sputtering-induced erosion. Not only do most materials have an unacceptably short service life as a result of sputtering, but the sputtered material enters the plasma and causes energy loss by line emission. Since the rate of energy loss is proportional to  $Z^3$ , high-Z refractory metals, which have low sputtering yields for light ion impact, are probably unacceptable because even very low plasma impurity levels of high-Z atoms are sufficient to quench the thermonuclear burn.

It has been proposed that the erosion of plasma-interactive components (e.g., first walls and limiters) in fusion devices and the plasma contamination resulting from entry into the plasma of eroded material might be significantly reduced through the use of materials which form a self-generating

**Keywords:** Lithium Alloys, Sputtering Properties, Surface Composition, Near-Surface Composition, Gibbsian Segregation, Radiation-Induced Segregation, Solid-State Diffusion, Ion Bombardment, Copper-lithium, Aluminum-lithium

### \*Address for Correspondence

Alan R. Krauss  
Argonne National Laboratory  
MSD/CHM-200  
Argonne, IL 60439  
Phone NO. (312) 972-3520

low-Z coating as a result of the interaction between the plasma and the surface. According to the results of the Monte Carlo computer code, TRIM, the low-Z coating need not be more than 1-2 atomic layers in thickness in order to very significantly reduce the sputtering yield of the higher-Z component [7]. If in addition, the low-Z material is sputtered primarily in the form of secondary ions, the loss of this component is also very low since the electric and magnetic fields of a magnetic fusion device trap secondary ions at the surface of the plasma-interactive component. The service life of such a material is determined by the concentration profile and the extent of depletion of the low-Z component.

It has been experimentally found that lithium spontaneously forms an overlayer in Al-Li and Cu-Li binary alloys [8], and that the lithium overlayer results in ~4-6x reduction in the sputtering yield of the solvent metal. Additionally, enhanced secondary electron emission has been observed [11] to result from the formation of the lithium overlayer. In a fusion environment, the plasma edge temperature, and consequently the sputtering rate of plasma-interactive components, may be reduced as a result of high secondary electron yields. The lithium, which is preferentially sputtered, would constitute the primary plasma impurity in a fusion device. Because of its low atomic number, it is expected that there would be negligible plasma energy loss due to line emission by lithium plasma impurities. The Al-Li and Cu-Li binary alloys are therefore plausible candidates for the production of self-sustaining lithium coatings as a means of reducing the substrate sputtering erosion yield in fusion devices.

Cu-Li alloys are of interest for fusion applications because copper has a higher melting point and better thermal conductivity than aluminum. Additionally, since copper has a higher work function than aluminum, lithium sputtered from a copper surface has a higher secondary ion fraction. Because of the electric and magnetic fields in a fusion environment, secondary ions are trapped at the surface and do not constitute a source of plasma impurities. There is also a long-term conditioning effect in the Cu-Li alloy which results in an ability to maintain the lithium overlayer for extended periods of time. An example of this effect is shown in Fig. 1 [6] for a Cu-6 at.% Li alloy sputtered by 100 eV He ions extracted from a plasma. The amount of copper in the plasma was determined by monitoring the intensity of the 303.6 nm Cu I emission line. The sputtering yield for pure copper was dose-independent, whereas the CuLi alloy exhibited a dramatic reduction in the amount of copper entering the plasma after extended sputtering.

Although the mechanism of this conditioning process is not fully understood, it appears to be related to radiation-induced precipitation of Cu-Li compounds [12]. The secondary ion fraction of the sputtered lithium varies significantly, depending on the material and experimental conditions [14,3] but has been found to be as high as 90% [2]. It is therefore relevant to determine the initial surface composition, time evolution, and steady state composition of the surface after prolonged sputtering. A detailed comparison is made between Cu-Li and Al-Li alloys.

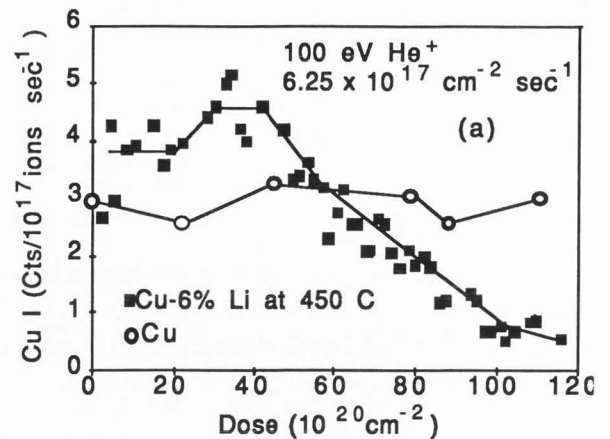


Fig. 1: Dose dependence of the 303.6 nm Cu I emission line (arbitrary units) for plasma sputtering of a pure copper sample (O) and Cu-6 at.% Li (■) by 100 eV He<sup>+</sup> at 450°C with a flux of  $6.25 \times 10^{17}$  ions  $\text{cm}^{-2} \text{sec}^{-1}$ .

### Theory

At thermal equilibrium, the composition of the first atomic layer of a binary alloy [26] is given by

$$C_{1a}/C_{1b} = C_a/C_b \exp(-\Delta H_s/kT) \quad (1)$$

where  $C_{1a}$  and  $C_{1b}$  are the first atomic layer concentrations of species  $a$  and  $b$ ,  $C_a$  and  $C_b$  are the bulk concentrations of  $a$  and  $b$ , and  $\Delta H_s$  is the heat of segregation, which is related to bond enthalpies, atom size, and the alloy crystal structure. During high temperature sputtering, the surface composition is altered as a result of radiation-enhanced diffusion, radiation-induced segregation, preferential sputtering and recoil mixing. At steady state, the surface composition is determined by preferential sputtering and is given by

$$C_{1a}/C_{1b} = C_a S_b / C_b S_a \quad (2)$$

where  $S_a$ ,  $S_b$  are the sputtering yields of species  $a$  and  $b$  in the alloy. Eq. 2 is based on the assumption that sputtered atoms originate entirely in the first layer. A number of recent experiments and calculations show that this is approximately true under the conditions to be discussed in this paper. Initially, there will be a transitory period during which large changes in the surface concentration and sputtering rate occur. The steady state condition (expressed by Eq. 2), however, will be reached only when the subsurface concentration of the segregating species has been depleted to a depth

$$\lambda = D_a / v \quad (3)$$

where  $v$  is the surface recession velocity and  $D_a$  is the radiation-enhanced diffusion coefficient of species  $a$ , defined as

$$D_a = d_{av} C_v + d_{ai} C_i \quad (4)$$

where  $d_{av}$ ,  $d_{ai}$  are the diffusivity coefficients for species  $a$  via vacancies and interstitials, respectively, and  $C_v$  and  $C_i$  are the vacancy and interstitial concentrations.

Radiation-induced segregation (RIS) results from a preferential coupling of either solute or solvent species with radiation-induced point defects, and can produce either a subsurface buildup or depletion of the solute species, depending on the relative magnitudes of the solute-defect and solvent-defect interactions. RIS depends on the defect concentration gradients; the flux of atomic species  $a$  across an imaginary plane is given by

$$J_a = -D_a \nabla C_a - C_a (d_{ai} \nabla C_i - d_{av} \nabla C_v). \quad (5)$$

In principle, both vacancies and interstitials affect the diffusion of the solute species  $a$  relative to the solvent  $b$ . However, in many alloys, RIS is dominated by one defect species or the other.

The model used to calculate the solute concentration profile resulting from all these processes has been described in detail elsewhere [9,16-18]. In order to define the quantities used in the present calculations, we note that for thermally activated diffusion via vacancy or interstitial coupling, the activation energies are given by

$$E_{av} = E_{fv} + E_{mv} \quad (6a)$$

$$E_{ai} = E_{fi} + E_{mi} \quad (6b)$$

where  $E_{fv}$ ,  $E_{mv}$ ,  $E_{fi}$ ,  $E_{mi}$  are the formation and migration energies for vacancies and interstitials, respectively. It is assumed in Eqs. 6a and 6b that only monovacancies are relevant: divacancies and higher order vacancies do not exist in sufficient numbers to affect the solute transport. During high temperature sputtering, the majority of the vacancies and interstitials are normally created by the radiation, and the movement of atoms in the solid is then determined by the migration energies, rather than by the activation energies. Such is the case for the Cu-Li alloy system. However, for the Al-Li system, the vacancy formation energy is low and the thermal equilibrium vacancy concentration is  $\sim 10^3$  times that of Cu-Li. Consequently, the thermally-induced vacancies dominate the radiation-induced vacancy concentration and  $\nabla C_v$  is therefore very small. Therefore vacancy-induced RIS is expected to be negligible. If RIS is significant in Al-Li, it must then be driven by interstitials. Additionally, the formation of solute-interstitial complexes modifies the solute concentration profile. These complexes are probably not stable at the temperatures to be discussed here, but they are continually created during the sputtering process and there are always some available. The concentration of solute-interstitial complexes is determined by the temperature and the solute-interstitial binding energy,  $E_{bi}$ . For each of the calculations presented in this paper, the values used as input are tabulated in Table 1.

**Table 1**  
**Input Parameters for the Calculation of Solute Concentration Profiles**

Fig.		$E_{mv}$	$E_{fv}$	$E_a$	$E_{mi}$	$E_{bi}$
2	Cu	0.82	1.20	2.02	0.117	
	Li	0.70	0.85	1.55	0.117	0
3a	Al	0.67	0.81	1.48	0.115	
	Li	0.63	0.77	1.40	0.115	0
3b	Al	0.63	0.81	1.48	0.115	0
	Li	0.63	0.77	1.40	0.150	0.101
4	Al	0.67	0.81	1.48	0.115	0
	Li	0.54	0.66	1.20	0.115	
9	Al	0.67	0.81	1.48	0.115	0
	Li	0.63	0.77	1.40	0.115	

For the Cu-Li system, the activation energy for the diffusion of lithium in copper via vacancy coupling is lower than that of copper in copper (Table 1). Consequently, lithium is expected to accumulate in regions of maximum damage density. The calculated Li concentration profile is shown in Fig. 2 for  $1.1 \times 10^4$  seconds of 1.7 keV  $D^+$  bombardment at 350 °C. There is a shallow lithium-rich layer right at the surface, followed by a region of extreme lithium depletion just below the surface. Starting at a depth of  $\sim 1$  nm, there is a broad region about 100 nm wide of very high lithium concentration. The shape of this subsurface region depends on temperature, and the mass and kinetic energy of the incident ion as well as the Li sputtering yield [12]. However, the general shape of the subsurface region of enhanced lithium concentration is related to the damage profile. If the damage profile is sufficiently peaked, it is expected [12] that the subsurface lithium concentration will exceed 20 at.% (shown in Fig. 2 by the dotted line) and precipitate the formation of  $Cu_4Li$ , the only known copper-lithium compound. Radiation-induced precipitation is expected to further alter the composition profile since precipitates may serve as additional defect sinks and/or solute traps. Consequently, the observed lithium profile will be broader than shown in Fig. 2.

For the  $\alpha$  phase of the Al-Li system, it is much harder to specify the effect of RIS. The activation energies for diffusion of the two component species by vacancy coupling and by interstitials have been measured experimentally. However, the interpretation of the experiments depends on the assumed lithium diffusion mechanism. The thermal activation energy for the diffusion of Li in Al is reported as 1.4 eV [25]. Using the rule, valid for vacancy-induced diffusion in FCC metals, that vacancy formation energy is 55% of the activation energy [20] gives  $E_{fv}(Li) = 0.77$  eV and  $E_{mv}(Li) = 0.63$  eV. Experimentally, a value  $E_{fv}(Al) = 0.76 \pm 0.04$  eV has been obtained by positron annihilation spectroscopy for the self-diffusion of Al

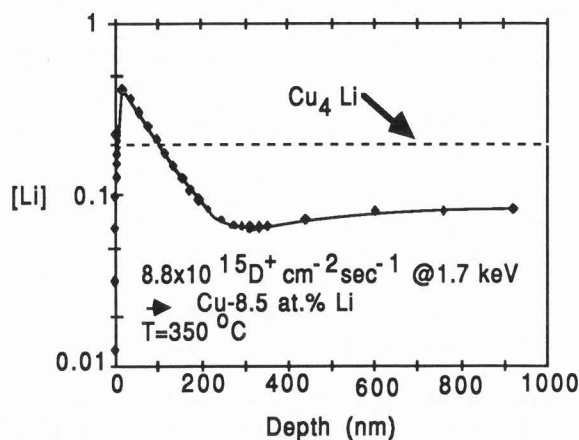


Fig. 2: Calculation of the lithium concentration profile of Cu-8.5 at.% Li bombarded by  $1 \times 10^{20}$  1.7 keV  $D^+$  at a flux of  $8.8 \times 10^{15} \text{ cm}^{-2} \text{ sec}^{-1}$  at  $350^\circ\text{C}$  for vacancy-driven RIS. The dashed line corresponds to the compound  $\text{Cu}_4\text{Li}$ .

[5], based on the assumption of a monovacancy model. However, it was found that a better fit to the temperature dependence of the diffusion coefficient could be obtained by assuming the existence of a divacancy mechanism. The formation energy of the lithium monovacancy was then found to be 0.66 eV and the divacancy formation energy was 0.3 eV.

In order to determine the role of interstitials in the solute diffusion in  $\alpha$  phase Al-Li, different values of solute migration energy ( $e_{\text{mia}}$ ) ranging from 0.115 eV (the migration energy of Al in Al via interstitials) to 0.25 eV were assumed. For a given value of solute-interstitial binding energy ( $e_{\text{bia}}$ ), the calculated lithium profiles were independent of  $e_{\text{mia}}$ . Varying  $e_{\text{bia}}$  for a given value of  $e_{\text{mia}}$  resulted in very slight change in the calculated lithium profiles for all values of  $e_{\text{bia}} \leq 0.1$  eV. It therefore appears that radiation-induced segregation by an interstitial mechanism is negligible compared with vacancy-related effects. This conclusion is also supported by the fact that at thermal equilibrium the vacancy concentration is 11 orders of magnitude larger than the interstitial concentration and during irradiation it is still up to 8 orders of magnitude larger. Consequently, large  $\text{VC}_i$  terms in Eq. 5 cannot be obtained and RIS by interstitials is not dominant. Since  $\text{VC}_v$  is also small, as discussed above, the solute flux in Eq. 5 is dominated by the  $\text{VC}_a$  term.

The model used here is based on the assumption that only monovacancies and interstitials affect the radiation-related transport properties [16-18]. Formation energies for the aluminum vacancy ranging from 0.73 eV to 0.81 eV were used to calculate the predicted lithium concentration profile. It was found that regardless of the value used for  $E_{\text{fv}}(\text{Al})$ , the best fit to the experimental data resulted when a value  $E_a(\text{Al})=1.48$  eV was used, regardless of the  $E_{\text{fv}}(\text{Al})$  value. This is again in accord with thermally-dominated diffusion processes. The results for  $E_{\text{fv}}=0.81$  eV are presented here.

Calculations have been performed for the Al-3.46 at.% Li system subject to 1.7 keV  $D^+$  sputtering for  $2.7 \times 10^4$  sec-

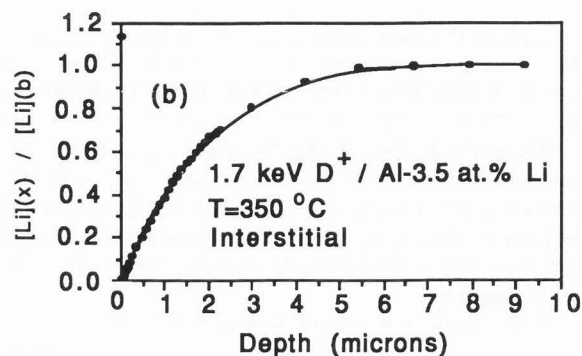
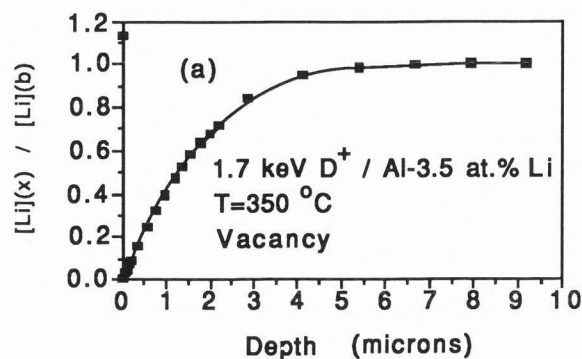


Fig. 3: Calculated lithium concentration profile (normalized to the bulk concentration) for 1.7 keV  $D^+$  bombardment of Al-3.5 at.% Li at  $350^\circ\text{C}$ . (a) Vacancy mechanism was assumed using 0.63 (1.4) eV for the lithium migration (activation) energies and 0.67 (1.48) eV for aluminum. (b) Interstitial mechanism was assumed using 0.15 eV for the lithium migration energy and 0.115 for aluminum.

onds. Two different mechanisms have been assumed. In one case, (Fig. 3a), a preferential vacancy exchange mechanism with  $E_{\text{mv}}(\text{Li})=0.63$  eV ( $E_a(\text{Li})=1.4$  eV) and  $E_{\text{mv}}(\text{Al})=0.67$  eV ( $E_a(\text{Al})=1.48$  eV) has been assumed. In the other case (Fig. 3b), preferential exchange or preferential association has been assumed between lithium and the interstitials, using values of  $E_{\text{mi}}(\text{Li})=0.150$  eV,  $E_{\text{mi}}(\text{Al})=0.115$  eV, and  $E_{\text{bi}}(\text{Li})=0.101$  eV, obtained from the literature [27]. Nearly identical Li profiles are obtained for the two mechanisms. It should be noted, however, that regardless of the mechanism assumed for the Al-Li system, the predicted solute concentration profile is qualitatively quite different from that of the Cu-Li system.

In the absence of strong RIS, the major radiation effects are preferential sputtering, radiation-enhanced diffusion (RED), and cascade mixing. Phenomenologically, it is possible to model these processes by a surface loss mechanism and an effective bulk diffusion rate. This model is formally equivalent to a thermal loss mechanism and has been used to characterize the loss of lithium from  $\alpha$  phase Al-Li by thermal evapo-

ration. Following the approach of Carlslaw and Jaeger [4], Schulte *et al.* [23] describe the lithium concentration profile by:

$$C_a(x) = C_1 + \frac{4(C_a - C_1a)}{\pi} \sum_{n=0}^{\infty} \frac{(1)^n}{(2n+1)} \exp\left(\frac{-D_a t (2n+1)^2 \pi^2}{4L^2}\right) \times \cos\left(\frac{(2n+1)\pi x}{2L}\right) \quad (7)$$

where  $D_a$  is given by:

$$D_a = D_0 \exp(-E_a/kT) \quad (8)$$

and  $L$  is the specimen thickness,  $C_a$  is the bulk concentration of a,  $C_a(x)$  is the depth-dependent concentration of a and  $C_1a$  is the surface concentration of a.  $E_a$  is again the sum of the defect formation and migration energies. For  $\alpha$  phase Al-Li, we have used the values  $D_0 = 3.292 \text{ cm}^2 \text{ sec}^{-1}$  and  $E_a = 1.4 \text{ eV}$  [23,25], although for very dilute alloys  $E_a$  has been reported to be as low as 1.2 eV [9].

For purely thermal processes, the lithium diffusion is characterized by Eq. 8 with constant  $E_a$  and  $D_0$  values. In a radiation environment, it is expected that the effective diffusion coefficient is depth-dependent. The exact shape of the profile depends on the near-surface lithium concentration. If it is assumed that the near-surface lithium depletion is nearly complete, the predicted solute concentration profile at 350°C with a constant activation energy of 1.4 eV is as shown in Fig. 4a. Except for the fact that the surface peak resulting from Gibbsian segregation is not considered in the treatment of Schulte *et al.* [23], this profile is similar to the profile expected for RIS for a vacancy coupling mechanism with an activation energy of 1.2 eV (Li migration energy of 0.47 eV) as shown in Fig. 4b.

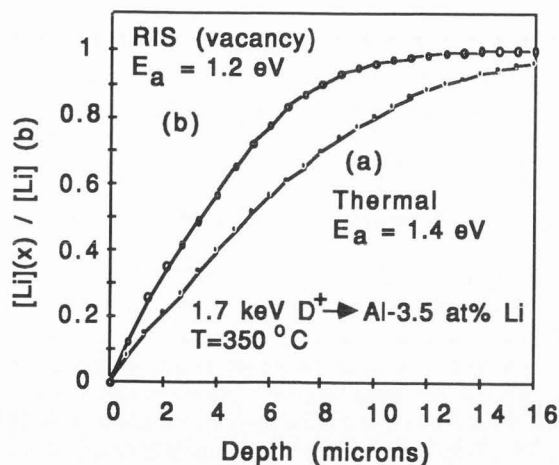


Fig. 4: (a) Carlslaw-Jaeger lithium profile calculation for Al-3.5 at.% Li at 350°C using  $E_a = 1.4 \text{ eV}$  and assuming lithium evaporates as soon as it reaches the surface. (b) Lam-Johnson calculation of the lithium profile for 1.7 keV  $D^+$  bombardment at a flux of  $8.8 \times 10^{15} \text{ cm}^{-2} \text{ sec}^{-1}$  for  $2.7 \times 10^4$  seconds, assuming vacancy-coupled RIS with  $E_a = 1.2 \text{ eV}$ .

For  $\beta$  phase (47-55 at.% Li) Al-Li alloys, it is appropriate to model the lithium concentration via a purely diffusional process since the diffusivity of lithium is  $\sim 4$  orders of magnitude greater than in the  $\alpha$  phase material [24]. The maximum sustainable lithium loss rate is determined by the requirement that the material remain in the  $\beta$  phase, i.e., the surface Li concentration does not drop below 47 at.%. This loss rate is determined by the bulk Li concentration  $C_a(b)$  and the temperature and is given by the first term on the right side of Eq. 5 where the gradient term may be approximated by:

$$\nabla C_a = (C_a - 0.47) N_a \lambda \quad (9)$$

where  $\lambda$  is defined by Eq. 3 and  $N_a$  is the average atomic density of  $\beta$  Li-Al. A detailed analysis of the service life of  $\beta$  Li-Al for fusion applications is presented elsewhere (A. B. DeWald, A. R. Krauss and N. Q. Lam, in preparation), but preliminary results indicate lifetimes which compare favorably with conventional materials.

### Experimental

Aluminum-lithium alloys were prepared by the Sumitomo Light Metal Industry, and the copper-lithium alloys were prepared at Argonne National Laboratory. The experimental details of the system used for  $D^+$  sputtering [21] are given elsewhere. Samples 3.2 cm<sup>2</sup> x 2 mm thick were mounted on a ceramic heater in a vacuum system with a base pressure  $\sim 2 \times 10^{-7}$  torr. The sample mount was placed inside a gridded current measuring cup at a distance of 36 cm from a Duo-Pigatron ion source. The chamber pressure was  $\sim 2 \times 10^{-4}$  torr when the ion source was operating.  $D_2$  was used as the feed gas and the dominant ion species was  $D_3^+$ . The grid closest to the sample was biased negatively to suppress secondary electron emission from the sample, and both instantaneous and integrated sample currents were measured. The sample was heated, typically to 350°C, and a beam consisting of  $8.8 \times 10^{15} \text{ cm}^{-2} \text{ sec}^{-1}$  1.7 keV  $D^+$  ions (5 keV  $D_3^+$ ) was allowed to impinge on the target for a predetermined time. The samples were then removed and weighed to determine the average lithium loss. The lithium concentration profile was determined at Nagoya University by Nuclear Reaction Analysis (NRA), using the  $^7\text{Li}(p,\alpha)\text{He}$  reaction. This technique is capable of quantitatively measuring the lithium concentration profile with a depth resolution of  $\sim 150 \text{ nm}$ .

Similar samples were analyzed using Auger and SIMS. These samples were sputtered at elevated temperature and the lithium and copper AES and SIMS signals were continuously monitored. A representative sampling of Cu-Li alloys was subjected to high flux plasma sputtering at the PISCES device at UCLA. These experiments are described in greater detail elsewhere [6,13].

### Results

Fig. 5 shows the NRA lithium profile for a Cu-8.5 at.% Li sample. In the as-prepared state (5a), the lithium con-

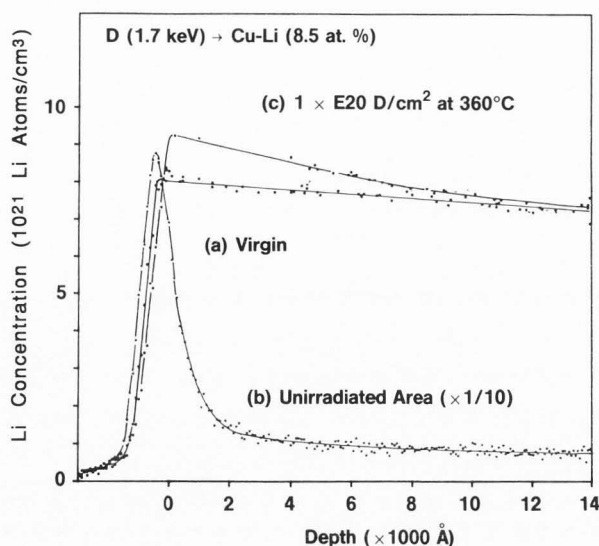


Fig. 5: NRA experimental lithium profile for Cu-8.5 at.% Li (a) as-prepared, (b) heated to 360°C for  $11.3 \times 10^3$  seconds. (c) bombarded at 360 °C to a dose of  $1 \times 10^{20}$  1.7 keV  $D^+$   $cm^{-2}$ . The dashed line corresponds to the compound  $Cu_4Li$ .

centration shows only a slight peaking at the surface: the concentration is nearly constant and equal to the bulk concentration of  $7.2 \times 10^{21}$  atoms/ $cm^3$ . The sample was then heated to 360°C and subjected to a dose of  $1 \times 10^{20}$  1.7 keV  $D^+$  ions at a flux of  $8.8 \times 10^{15}$   $cm^{-2} sec^{-1}$ . The edge of the sample was under a protective mask and received no bombardment. In this area (5b), NRA reveals a lithium-rich surface layer. The apparent width of this peak is limited by the depth resolution of the NRA technique, but the Li signal corresponds to a Li layer thickness  $\sim 100$  monolayers thick ( $1.4 \times 10^{17}$   $cm^{-2}$ ). In the irradiated area (5c), there is a region of increased subsurface lithium concentration as predicted by the calculation of Fig. 2. As predicted, the experimental profile is slightly broader than the calculated profile although the qualitative agreement between Figs. 2 and 5 is excellent.

For the Al-3.46 at.% Li sample, a brief cleaning consisting of  $Ne^+$  sputtering and heating to 350°C for 150 seconds resulted in the formation of a surface Li peak (Fig. 6a). Prolonged heating ( $8.1 \times 10^4$  seconds) resulted in an increase of the surface peak, but there was no evidence of subsurface depletion. When the sample was pre-irradiated with a dose of  $1 \times 10^{20}$  1.7 keV  $D^+$  / $cm^2$  (Fig. 6b), an initial lithium surface peak was again observed although it was smaller than that of Fig. 6a. However, subsurface depletion was observed to a depth substantially greater than that of the ion-induced damage. Continued heating of the pre-irradiated sample resulted in both an increase in the surface peak and the disappearance of the subsurface depletion region.

The effect on the sputtering yield of the aluminum is shown in Fig. 7. Sputtering yields were measured by weight loss methods. Heating to 200°C during sputtering by a flux of  $8.8 \times 10^{15}$   $D^+$   $cm^{-2} sec^{-1}$  resulted in only a slight reduction in

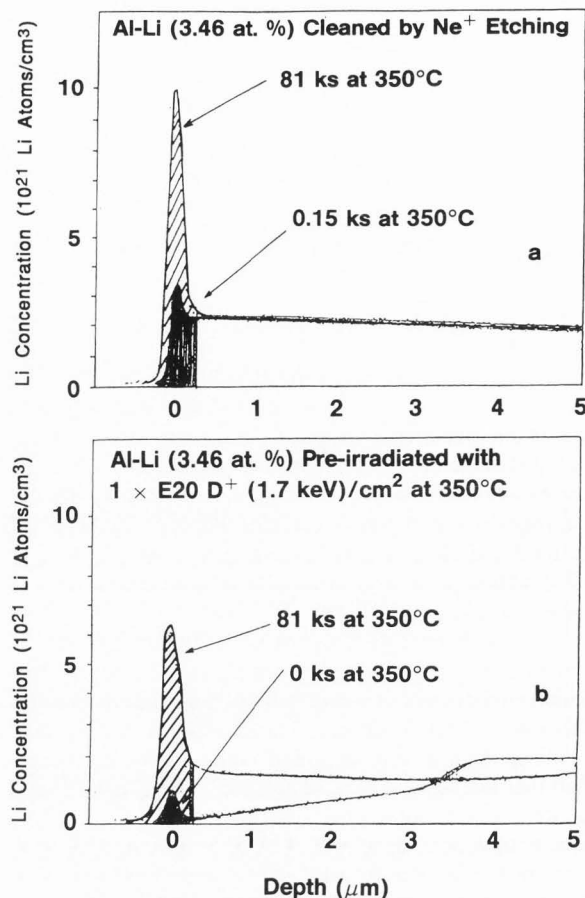


Fig. 6: Experimental lithium profile for Al-3.46 at.% Li after heating for two different times and cleaning by  $Ne^+$  etching (upper curve) and pre-irradiation by 1.7 keV  $D^+$  to a dose of  $1 \times 10^{20}$   $D^+$ / $cm^2$  (lower curve).

the aluminum yield. Heating to 350°C resulted in a greater initial decrease in the aluminum yield, followed by a progressive increase. Heating to 400°C resulted in a still greater initial reduction of the aluminum yield ( $\sim 2x$ ), but a more rapid increase to the pure aluminum value. For bombardment at 350°C by 1.7 keV  $D^+$  to a dose of  $2.4 \times 10^{20}$   $cm^{-2}$ , it was found that the aluminum sputtering yield had returned to 87% of the value for elemental Al. It should be noted, however, that although Fig. 7 qualitatively demonstrates aspects of the change in sputtering yield, the experimental results vary significantly from one sample to the next [22].

The reason for this behavior can be understood in terms of the lithium concentration profiles shown in Fig. 8. Curves (a) and (b) show the effect of raising the temperature from 200 to 350°C. Because of the greater lithium diffusivity, the depletion extends to greater depth at the higher temperature. Comparing curves (b) and (c), increased dose also results in depletion to a greater depth. Curve (d) shows extreme depletion at high dose and high temperature. These results are similar to results previously reported for the high flux sputtering of Cu-Li alloys [13]. In both the Cu-Li and Al-Li systems, reduced loss of the solvent atoms occurs only when the lithium

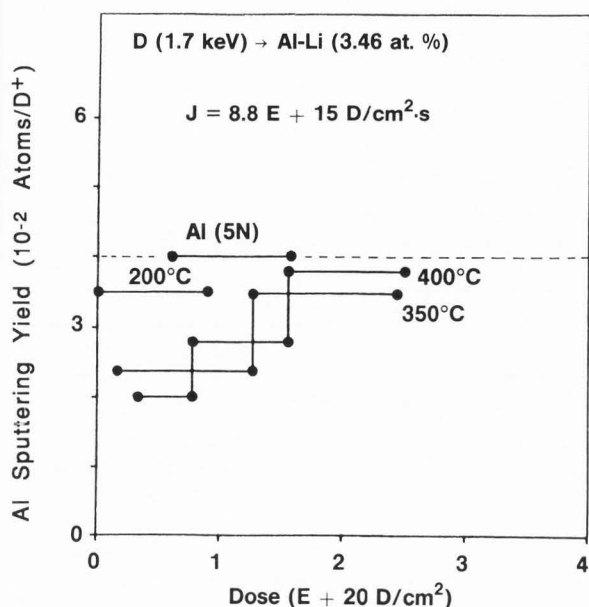


Fig. 7. Aluminum sputtering yield for Al and Al-3.46 at.% Li at 200, 350 and 400°C subject to bombardment by 1.7 keV  $D^+$  as a function of dose. Measurements performed by RBS of Si catcher foil.

segregates rapidly enough to maintain an overlayer. However, rapid segregation to the surface also produces greater subsurface lithium depletion as a result of preferential sputtering.

The shape of the lithium profiles in Fig. 8 may be analyzed for information concerning the diffusion process. Fig. 9a shows the experimental profile corresponding to Fig. 8c, the calculation for vacancy-driven RIS, and the calculation for thermal diffusion loss from Fig. 4a. The experimental curve lies between the two calculated curves and is characterized by a near-surface "toe" not predicted theoretically. As a means of phenomenologically incorporating radiation-enhanced diffusion in the thermal diffusion model, it may be assumed that the diffusion coefficient varies with depth. It is generally known that vacancy migration results in enhanced diffusion at depths much greater than the ion damage range and may extend to several microns [18]. Empirically a much better fit to experiment is found by using a thermal evaporation model, assuming a surface lithium concentration of 0.001, and a reduced activation energy of 1.3 eV near the surface, extrapolating linearly to a 1.4 eV bulk value at a depth of 4 microns (Fig. 9b).

### Summary

Thermal segregation, radiation-enhanced diffusion, preferential sputtering, and radiation-induced segregation can significantly alter the surface composition, sputtering properties, and concentration profile of alloys undergoing high temperature sputtering. The steady state surface composition is

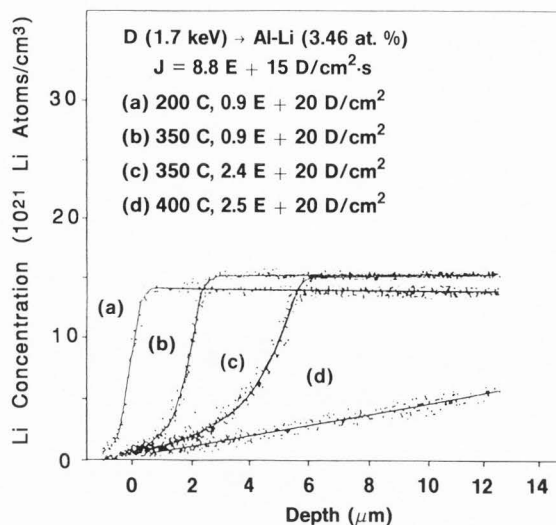


Fig. 8. Lithium concentration profile for Al-3.5 at.% Li subjected to a flux of  $8.8 \times 10^{15} D^+ cm^{-2} sec^{-1}$  at 1.7 keV for various doses and sample temperatures.

determined by preferential sputtering, but for some systems in which radiation-induced precipitation occurs (Cu-Li), or in which the depletion depth exceeds the component thickness ( $\beta$  Al-Li), steady state conditions are not expected to be reached in practice and the solvent sputtering rate may be kept below the value corresponding to the bulk stoichiometry. For other systems ( $\alpha$  Al-Li), there is subsurface depletion and consequent inability to maintain a Li-rich surface layer. However, even in this case, both the Li surface layer and the Li depth profile can be restored to nearly the original state by continued heating. This finding is significant for applications where surface removal is pulsed but the sample is maintained at elevated temperature between pulses (A. B. DeWald, A. R. Krauss and N. Q. Lam, in preparation)<sup>28</sup>.

For the copper-lithium system, substantial radiation-induced segregation occurs as a result of the vacancy mechanism. Consequently, there is a subsurface region of enhanced lithium concentration. The lithium concentration may exceed the solubility limit, causing radiation-induced precipitation of a lithium-rich compound,  $Cu_4Li$ , and consequently there is some broadening of the solute concentration profile. For the aluminum-lithium system, the solute concentration profile corresponds to extensive sub-surface lithium depletion. The experimental width of the depletion region is in accord with calculations based on literature values for migration and activation energies. The calculated shape of the profile however, is dominated by vacancy mechanisms and is nearly independent of assumed interstitial migration energies. Because of the high concentration of thermal equilibrium vacancies, vacancy-induced diffusion depends on the activation energy rather than the vacancy migration energy. The shape of the experimental lithium depth profile is somewhat different from that calculated on the basis of parameter values which are depth-independent. A

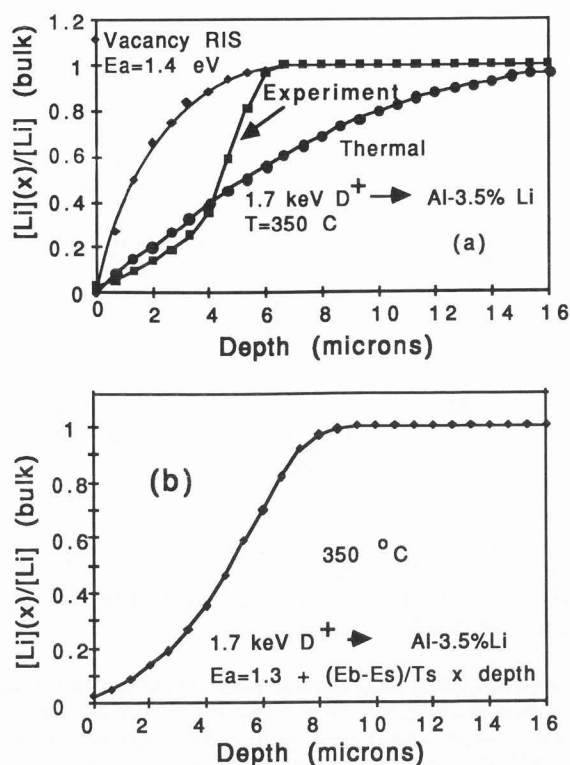


Fig. 9: (a) Experimental lithium concentration profile for Al-3.5 at.% Li bombarded by  $8.8 \times 10^{15}$  D<sup>+</sup> cm<sup>-2</sup> sec<sup>-1</sup> for  $2.7 \times 10^4$  sec at 350°C (■), combined radiation effects model calculation assuming RIS proceeds via vacancy migration, using  $E_a = 1.4$  eV (◆), thermal loss model using  $E_a = 1.4$  eV, independent of depth (●). (b) Thermal loss model assuming  $E_a = 1.3$  eV at the surface and increases linearly with depth to the 1.4 eV bulk value at a depth of 4 μm.

much better fit to the experimental Li concentration profile can be calculated if it is assumed that the activation energy for radiation-enhanced diffusion of lithium in aluminum is depth-dependent.

#### Acknowledgement

This work was supported in part by the U.S. Department of Energy, BES-Materials Sciences, under Contract W-31-109-ENG-38, and a grant of computer time at the Energy Research Cray XMP and Magnetic Fusion Cray computers at the Magnetic Fusion Energy Computing Center.

#### References

- [1] Abe K, Yoshizawa I, Kamada K, Kayano H (1986). Mechanical properties and microscopic structure of Al-Mg alloys after 14 MeV neutron irradiation. *J. Nucl. Mater.* **141-143**, 915-920.
- [2] Barth H, Muehling E, Eckstein W (1986). Investigation of a copper-lithium alloy as a possible first wall and limiter material in fusion devices. Max Planck Institut fur Plasmaphysik IPP 9/58, March 1986, 1-11.
- [3] Bohdanský J, Roth J (1987). Temperature dependence of sputtering behavior of Cu-Li alloys. *Nuclear Instr. Meth.* **B23**, 518-520.
- [4] Carlslaw HS, Jaeger JC (1959). *Conduction of Heat in Solids*, 2nd ed. 1959, Oxford University Press, p. 97.
- [5] Fluss MJ, Berko S, Chakraborty B, Lippel P, Siegel RW (1984). Positron annihilation spectroscopy of the equilibrium vacancy ensemble in aluminum. *J. Phys. F.* **14**, 2855.
- [6] Goebel DM, Hirooka Y, Conn RW, Leung WK, Campbell GA, Bohdanský J, Wilson KL, Bauer W, Causey RA, Pontau AE, Krauss AR, Gruen DM, Mendelsohn MH (1987). Erosion and redeposition of materials in the PISCES facility. *J. Nucl. Mater.* **145**, 61-70.
- [7] Gruen DM, Krauss AR, Pellin MJ (1985). Effects of monolayer coverages on substrate sputtering yields. *Radiation Effects* **89**, 113-128.
- [8] Gruen DM, Krauss AR, Susman S, Venugopalan M, Ron M (1983). Gibbsian and radiation-induced segregation in Cu-Li and Al-Li alloys. *J. Vac. Sci. Technol.* **A1**, 924-928.
- [9] Kamel R, Ali AR, Farid Z (1978). Annealing spectrum of cold-worked dilute Al-Li alloys. *Phys. Stat. Sol.* **45**, 419-422.
- [10] Kawamura T, Amano T, Sagara A, Miyahara A (1984). Effect of the first wall condition on the start-up of the tokamak discharge. *J. Nucl. Mater.* **128&129**, 838-840.
- [11] Krauss AR, Auciello O, Uritani A, Valentine M, Mendelsohn M, Gruen DM (1987). Charge transfer processes and sputtering processes of self-sustaining alkali metal coatings on metal surfaces. *Nucl. Instr. Meth.* **B27**, 209-220.
- [12] Krauss AR, DeWald AB, Gruen DM, Lam NQ (1985). Synergistic sputtering properties of binary alloys. *Radiation Effects* **89**, 129-148.
- [13] Krauss AR, Gruen DM, Mendelsohn MH, Conn RW, Goebel DM, Hirooka Y, Leung WK (1987). High plasma flux elevated temperature sputtering of Cu-Li alloys. *J. Nucl. Mater.* **145**, 401-407.
- [14] Krauss AR, Mendelsohn MH, Gruen DM, Conn RW, Goebel DM, Hirooka Y, Leung WK, Bohdanský J (1987). Temperature and composition dependence of the high flux plasma sputtering yield of Cu-Li binary alloys. *Nuclear Instr. Meth.* **B23**, 511-517.
- [15] Lagues M, Domange JL, Hurault JP (1973). Segregation of dissolved Li to the surface of Si: a new activation process. *Sol. St. Comm.* **12**, 203-206.

[16] Lam NQ, Wiedersich H (1981). Modifications of subsurface alloy composition during high-temperature sputtering. *J. Nucl. Mater.* 103/104, 433-437.

[17] Lam NQ, Wiedersich H ((1982). Ion bombardment-induced subsurface composition modifications in alloys at elevated temperatures. *Rad. Eff. Lett.* 67, 107-112.

[18] Lam NQ, Wiedersich H (1987). Bombardment-induced segregation and redistribution. *Nucl. Instr. Meth.* B18, 471.

[19] McCoy LR, Lai S (1976). Lithium-silicon electrodes for the lithium-iron sulfide battery. Proceedings of the Symposium and Workshop on Advanced Battery Research and Design, Argonne National Laboratory, March 22-24, 1976 ANL-76-8, p. B167-B173.

[20] Ortega J (1982). Self-diffusion in FCC metals: correlation between melting temperature and vacancy parameters. *Z. Metallkund* 73, 665

[21] Sagara A, Kamada K (1986). Production of high-flux beams of hydrogen ions below 1 keV. *Jpn. J. Appl. Phys.* 25, 506-507.

[22] Sagara A, Kamada K (1986). Nagoya Institute of Plasma Physics 1985-1986 Annual Review ISSN 0547-1567, p. 97, Nagoya, Japan.

[23] Schulte RL, Papazian JM, Adler PN (1986). Application of nuclear reaction analysis to the investigation of lithium loss in the surface of Al-Li alloys. *Nucl. Instr. Meth.* B151, 550-554.

[24] Wen CJ, Boukamp BA, Huggins RA, Weppner W (1979). Thermodynamic and mass transport properties of "LiAl." *J. Electrochem. Soc.* 126, 2258-2266.

[24] Wen CJ, Boukamp BA, Huggins RA, Weppner W (1979). Thermodynamic and mass transport properties of "LiAl." *J. Electrochem. Soc.* 126, 2258-2266.

[25] Williams DB, Eddington JW (1974). Microanalysis of Al-Li alloys containing fine  $\delta'$  ( $Al_3Li$ ) precipitates. *Phil. Mag.* 30, 1147-1153.

[26] Wynblatt P, Ku RC (1977). Surface energy and solute strain energy effects in surface segregation. *Surf. Sci.* 65, 511-531.

[27] Young FW (1978). Interstitial mobility and interactions. *J. Nucl. Mater.* 69&70, 310-330.

[28] DeWald A. B., Krauss A. R. and Lam N. Q. (1988) Analysis of Self-Regenerating Coatings for Pulsed-Mode Fusion Plasma Operation. *J. Vac. Sci. Technol. A* (in press)

Editor's Note: All of the reviewer's concerns were appropriately addressed by text changes, hence there is no Discussion with Reviewers.